IJE TRANSACTIONS A: Basics Vol. 37 No. 04, (April 2024) 804-817

International Journal of Engineering

Journal Homepage: www.ije.ir

Computational Framework Development to Investigate Al Matrix with Low-Velocity Impact Behavior at Varied Temperatures for Cold Spray Composite Coating Design: Al/TiN Case

P. Chupong, K. Tuchinda*

Mechanical Engineering Simulation and Design Mechanical and Automotive Engineering, The Sirindhorn International Thai-German Graduate School of Engineering, King Mongkut's University of Technology North Bangkok, Thailand

PAPER INFO

Paper history:
Received 11 September 2023
Received in revised form 09 October 2023
Accepted 27 November 2023

Keywords:
Cold Spray
Low-pressure Cold Spray
Finite Element
Aluminum Particle
Hardened SKD11

ABSTRACT

Cold spray (CS) with Metal matrix composite (MMC) is an alternative process for improving surface properties, which is crucial in plastic manufacturing. Understanding of particle behavior during impact is required for CS. This study focused on developing a simplified computational framework using the single-shot particle impact model to predict the adherence of matrix particles in the low-velocity impact. In this work, the hardened SKD11 coated with Al matrix/TiN reinforcement composite was selected, aiming to verify the proposed framework. Al particle impact at different temperatures (300K, 623K, and 723K) under the low-velocity range of 350–600 m/s were simulated, revealing the particle temperature affects the cohesive area. As the particle temperature increases, the areas also increase under similar velocity. The flattening ratio was calculated from the simulation and found to be influenced by the particle velocity. The CS of pure Al and Al/TiN (75:25 wt.%) on the hardened SKD11 under 623K and 723K was carried out under the experiment with the estimated pressure based on the flattening ratio and particle behavior. The results suggest the coatings could be developed using estimated pressure. Al/TiN coating was deposited at different initial particle temperatures. Results reveal that low coating porosity (<0.01%) could be obtained for both cases, and the higher particle temperature reveals higher thickness and %porosity, which agree well with the computational results. The developed framework shows high potential for designing CS for MMC coating, provided the reinforcement particles do not significantly affect the matrix particle flow or impact conditions.

***doi**: 10.5829/ije.2024.37.04a.18*

Graphical Abstract

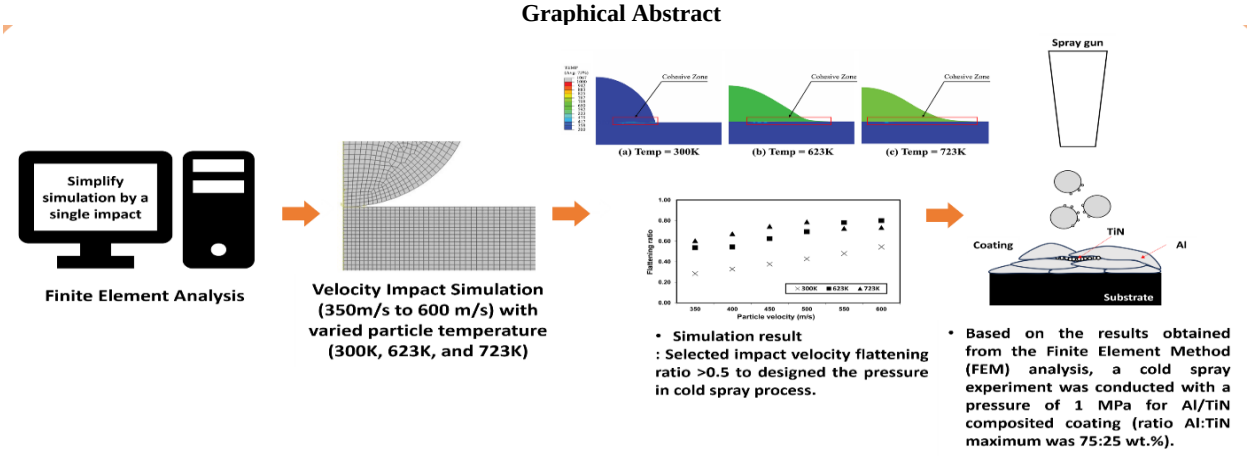

*Corresponding Author's email: karuna.t@tggs.kmutnb.ac.th (K. Tuchinda)

Please cite this article as: Chupong P, Tuchinda K. Computational Framework Development to Investigate Al Matrix with Low-Velocity Impact Behavior at Varied Temperatures for Cold Spray Composite Coating Design: Al/TiN Case. International Journal of Engineering, A: Basics. 2024;37(04):804-17.

1. INTRODUCTION

Steel is a versatile material with extensive applications across various industries. SKD11 holds an outstanding position in the production of plastic molds. One commonly employed method for enhancing material properties is heat treatment. Surface treatment is a step in the heat treatment process that increases surface properties and extends the materials' lifetime. Surface heat treatment involves various methods, such as nitriding, which can make the material's surface harder and increase wear resistance. Moreover, surface heat treatment processes such as physical vapor deposition (PVD), cathode arc physical vapor deposition (CAPVD), chemical vapor deposition (CVD), and plasma-assisted chemical vapor deposition (PACVD) are actively employed. These techniques use various coating materials, including AlCrN, CrN, TiAlN, TiC, AlTiN, and TiN, to augment the surface properties of molds. The heat treatment process enhances material properties and can also be employed to regenerate carbon and glass fibers from waste composites. While surface heat treatment offers numerous advantages in terms of improved properties, it also has the drawback of potential distortion due to the high temperatures exceeding 700°C or the long duration of the process (1-5). Another method involves applying a different material as a coating on the substrate's surface without allowing diffusion between the two layers. These methods offer rapid improvements, such as thermal spray, cold spray, and cold plasma. Thermal spray techniques, including flame spray and plasma spray, are widely employed for applying surface coatings. These processes involve the controlled melting of deposited particles onto the substrate (6, 7). In addition, the sacrificial anodes for cathodic protection method are widely used to protect steel from chloride attack (8). The cold spray (CS) coating was initially developed in the mid-1980s, which uses a high velocity and low temperature for solid powder, impinges on the substrate, and creates a surface coating (9).

Cold spray is a new branch of surface engineering that relates to surface improvement by applying powder particle coating on a substrate with high velocity (300–1200 m/s) through a de Laval nozzle at a temperature below the melting point of the spray material. At or above a critical velocity of particles, the particle plastic deformation rate suggests adherence of deformation particles on the substrate and with each other to form the coating. Critical velocity is the lowest velocity at which solid particles impinge or deform on the substrate. The critical velocity varies for each solid powder due to particle density and specific heat (10-13). The CS process typically uses 5–50 m powder particles. The CS had two categories, High-pressure and Low-pressure, at typical stagnation pressure ranges of 2–5 MPa and 0.3–1 MPa, respectively. High-pressure cold spray (HPCS) typically generates particle velocities of 800-1400 m/s using higher-density particles. The lower gases, such as nitrogen or helium, are the preferred propellant gases in this system. The low-pressure (LPCS) system generates particle velocities of 300–600 m/s and uses lighter-density particles; air or nitrogen allow propellant gases (14-16). In addition, particle velocity depends on particle size, density, and morphology. HPCS and LPCS processes for coating formation include two stages: particle-substrate and particle-particle interaction. The HPCS process bonding mechanism has a high particle velocity that allows for adiabatic shear band formation and bonding at the interface. For the LPCS process, the bonding mechanism is followed by i) breaking the oxide film by preliminary particle impact, ii) impact particle consolidation, and iii) densification from deformation and consolidation of particle collection due to the shot peening effect (17). The material particles generally use cold spray processes such as Al, Ti, Ni, Mg, etc. Because the properties of these materials can improve the wear and corrosion resistance of substrate materials, they are easy to deposit on substrates. However, these materials had limited mechanical properties, like Al, which can be susceptible to corrosion by galvanic or wear by abrasives (18-21). To improve the mechanical and physical properties of the base material particles, a metal matrix composite coating could be considered to increase hardness, wear resistance, and corrosion resistance.

The ceramic particles or hard particles used for reinforcement of the material included TiN, Al_2O_3, SiC, etc. Al, Cu, and Ni are widely utilized for matrix particles. The complex particle only peens on the layers or is embedded in a soft matrix (22). Al-based MMC with TiN by HPCS increases deposit hardness, has a low friction coefficient, and has a low wear rate compared to Al5356. TiN has higher hardness, electrical, and optical properties (23-25).

The computational technique, i.e., finite element method (FEM), could be used to study the effect of impact velocity on particle impact associated with the CS process. The model could be used for investigation of the particle characteristics after impinging, predicting critical velocity, predicting temperature between cohesion zones, predicting porousness in the coating, etc. (26-36). To comprehend adiabatic shear and plastic flow localization, it is crucial to recognize these phenomena as major contributors to particle/substrate bonding during the cold spray process. The flattening ratio serves as an indicator of the extent of particle deformation resulting from the impact, and it can provide valuable guidance for selecting the appropriate process pressure.

The objective of this study is to develop a simplified computational framework to predict the adherence of MMC coating by focusing on soft matrix. The results could be useful in the design of the CS process conditions to develop a specific MMC coating to improve the

surface properties of substrate material. SKD11 material with an Al/TiN coating was selected due to the high potential of Al/TiN coatings in protecting against thermal oxidation on the substrate. FEM was used as a tool to understand the deformation behavior of matrix particles, i.e., Al particles, on hard substrates. The effect of particle temperature and impact velocity was investigated. The impact of a single Al particle was modeled to investigate its behavior. It is expected that the behavior of single particle impact is sufficient to select a critical velocity that identifies the process temperature and pressure associated with obtaining Al/TiN coating, provided that the CS equipment performance is known. Notably, it is assumed that the presence of TiN particle does not significantly affect the Al particle flow or impact conditions. Experimental work was carried out to verify the technique proposed. The CS of pure Al coating and Al/TiN coating with different Al:TiN ratios were studied.

In this paper, the model descriptions are presented in the second section, providing a comprehensive overview of the theoretical framework. The third section covers experiment details, offering insights into the practical aspects of the study. The fourth section presents and discusses the computational results. The fifth section is dedicated to the discussion of the cold spray experiment results. Finally, the paper concludes in the last section, summarizing the key findings and their implications.

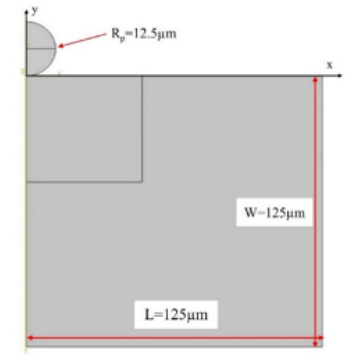

(a) 2D axisymmetric model

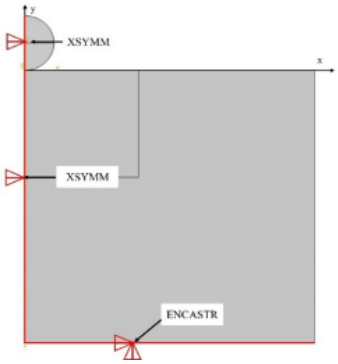

(b) boundary condition

Figure 1. Schematic diagram

2. MODEL DESCRIPTION

2. 1. Finite Element Modeling The study of a single CS particle's behavior upon impacting a substrate was conducted employing the widely used FEM software, ABAQUS/Explicit version 2017, which has seen extensive utilization in CS research (29-35). The model was simplified as a two-dimensional (2D) axisymmetric model was used for Arbitrary Lagrangian–Eulerian (ALE) analyses to simulate the large deformation processes that would occur during particle impact, with R representing radius, L representing length, and W representing width. The subscript p was assigned to distinguish the particle, as shown in Figure 1(a). Considering the axisymmetric nature of the normal impact process, the boundary conditions employed involved fixing the bottom of the substrate with the constraints (U1=U2=U3=0). and XSYMM, signifying symmetry about a plane X, as illustrated in Figure 1(b). The thermal and mechanical effects were assessed using two procedures available in ABAQUS: the Coupled Temperature Displacement procedure and the Dynamic Temperature Displacement Explicit procedure. Given the requirement for handling large deformations, the Dynamic Temperature Displacement Explicit procedure was deemed more suitable for this study. Accordingly, it was utilized to investigate the adiabatic stress effect (29).

For 2D, the particle/substrate interaction was executed by using the surface-to-surface contact (Explicit) penalty contact algorithm, choosing balance master-slave weighting contact for two element-based deformable surfaces that contact each other, and a finite sliding formulation (general and allows any arbitrary motion of the surfaces). The penalty contact algorithm aims to balance the weighting of forces on both the master and slave contact surfaces. In cold spray impact, the particle surface and substrate surface begin to slide relative to each other. The kinematic friction coefficient (μ_k) should be used instead of the static friction coefficient (μ_s) and is generally lower than μ_s. The friction coefficient (μ_k) was set to be 0.3 (29). The time increment used for this study was 60 ns. The particle velocity varied from 350 to 600 m/s for low-pressure cold spray. The initial substrate temperature was 300K, while particle temperature varied at 300K, 623K, and 723K.

The element type CAX4RT (A 4-node thermally coupled axisymmetric quadrilateral, bilinear displacement and temperature, reduced integration, and viscoelastic hourglass control) was used for the study, as shown in Figure 2. The meshing size at the contact between the particles and substrate was 0.5 μm for 25 μm particles (a meshing resolution of $1/50D_p$). To reduce resulting computational errors, Arbitrary Lagrangian–Eulerian (ALE) adaptive remeshing was performed to avoid mathematical truncation errors due to substantially

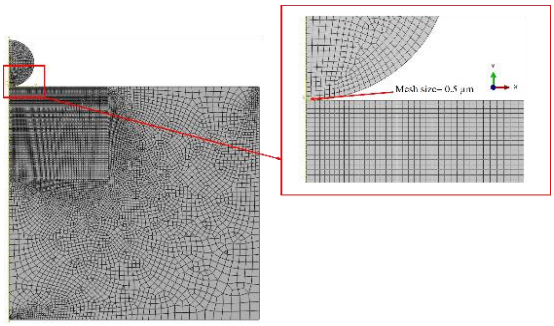

Figure 2 Mesh structure of 2D axisymmetric model

deformed elements [29]. This method was used to remesh the model 100 times in each increment.

2. 2. Materials Properties The numerical model uses the Johnson-Cook plasticity model to estimate the effects of strain-hardening, strain-rate hardening, and the equivalent flow stress, which can be expressed as follows (26):

$$\sigma = [A + B\varepsilon_p^n][1 + C\ln(\dot{\varepsilon}_p / \dot{\varepsilon}_0)][1 - (T^*)^m] \quad (1)$$

where σ is the flow stress, ε_p^n and $\dot{\varepsilon}_p$ are the equivalent plastic strain and strain rate, respectively, and $\dot{\varepsilon}_0$ is normalized reference strain rate. The constant A is yield stress, B is the strain-hardening parameter, C is strain-rate hardening, n is the power exponent of strain hardening, and m is the thermal softening constant. T^* is normalization temperature defined as follows:

$$T^* = \begin{cases} 0; & T < T_{trans} \\ (T - T_{trans})/(T_{melt} - T_{trans}); & T_{trans} \le T \le T_{melt} \\ 1; & T_{melt} < T \end{cases}$$

where T_{trans} is a reference transition temperature at or below which there is no temperature dependence of the response, and T_{melt} is the melting temperature. All constant parameters depend on materials and are shown in Table 1.

TABLE 1. Material properties used in FE mode (26, 31)

Parameters	Al	SKD11
Density (kg/m^3)	2710	8400
Young's modulus (GPa)	68.9	208
Poison's ratio	0.33	0.30
Heat capacity (J/kg.K)	904	461
Melting temperature (K)	916	1733
A (MPa)	148.4	1766
B (MPa)	345.5	904
n	0.183	0.39
C	0.001	0.012
m	0.895	3.38
Reference temperature (K)	293	298
Reference strain rate (s^{-1})	1	1

3. EXPERIMENT

3. 1. Materials and Deposition Process First, the cold spray (CS) of pure aluminum (Al) was carried out at 1 MPa, at a temperature of 623K (supported by Impact-Innovations GmbH in Germany) with an Impact spray machine model 5/11. Nitrogen was used as an accelerating gas with a 30 mm stand-off distance and a nozzle travel speed of 20 mm/s. Pure Al coating was deposited with a 3-pass process. The discussion of CS conditions will be provided in a subsequent text.

For the metal matrix composite coating experiment, TiN particles (0.8-1.2 μm, H.C. STARCK, USA) with spherical shapes for feedstock powders were used to produce TiN reinforcement in Al coating. Figure 3 presents the morphologies of Al-mixed TiN particles. The particles were mechanically mixed for 8 hours for deposition at an Al:TiN ratio of 75:25 wt.%, following the work of Wen-Ya Li (23). The low cold spray system installed at the University of the Witwatersrand, South Africa (Centreline, Center Line model SST PX, Canada) was used for composite coating development in this work. Low-pressure compressed air was used as an accelerating gas at 1 MPa with a 30 mm stand-off distance with deposition temperatures of 623K and 723K. A nozzle traveling speed of 12 mm/sc was employed to minimize porosity, as suggested by preliminary tests.

3. 2. Characterization The cross-section microstructure of the deposited coating was examined by scanning electron microscopy (SEM) (JSM 6610LV, JEOL, Japan), including an energy-dispersive X-ray spectroscope (EDS) (INCA-xart, Oxford, UK). The average percentage of particles and voids were evaluated using IMAGE J analysis with SEM imagery. The X-ray diffraction pattern was identified by X-ray diffraction (XRD) (SmartLab, Rigaku, Japan) analysis with Cu $K\alpha_1$ radiation under the condition of 40 kV and 30 mA in 30-80° scanning 2θ ranges and incidence angle of 0.5°. The microhardness of the top surface was tested by Vickers hardness indenter (SINOWON, China) with a load of 100 gf and a holding time of 15 s. Ten measurements on the polish cross-section were averaged to determine the average surface hardness. Note that this preliminary study did not include adhesive strength testing.

4. COMPUTATIONAL RESULTS AND DISCUSSION

4. 1. Effect of Particle Impact Velocity and Particle Temperature on Deformation Behavior The initial energy of particles with different impact velocities

predicted by the computational model is shown in Figure 4. The graph shows that increasing the particle velocity increases the kinetic energy. The energy transfer from the particle to the substrate was observed when the particle initiated contact with the substrate at 10 ns. Later, at approximately 30 ns, the particle deformation process starts, and the particle adheres to the substrate as there is insufficient energy for the particle to rebound.

The deformation of particles during impact could also be predicted. Figure 5 shows the typical results of equivalent plastic strain (PEEQ) distribution for different impact particle velocities at a constant initial temperature of 623 K (process temperature). The results show that particles will stretch out when the impact velocity is increased, eventually forming a sheet-like shape that adheres to the substrate. Hence, a certain particle velocity called critical velocity is required for the coating to be deposited successfully. At the contact surface, a metal "surface-scrubbing" jet is created. The lack of separation between the powder particle and the substrate at the contact surface suggests that there was no rebound or detachment of the particles from the substrate because of the impact. This agrees with work on critical velocity previously reported for Al on the hard substrate [30]. Further, a jetting phenomenon for 300 K starts at the edge of the particle at an impact velocity above 500 m/s.

In theory, the critical velocity may be described using particle temperature and material properties following Equation 2 for known material (28). Notably, the equation does not include the effect of the substrate material. This equation is used for estimating the critical velocity of soft particles on a soft substrate, the reference material, i.e.:

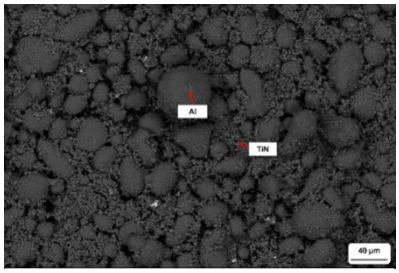

Figure 3. SEM micrograph of Al mixed TiN

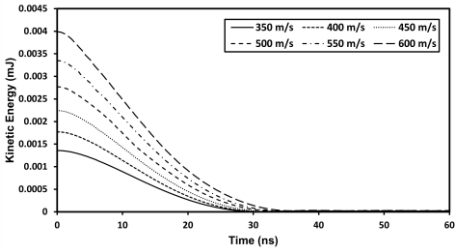

Figure 4. Kinetic energy of Al impact at varying impact velocity

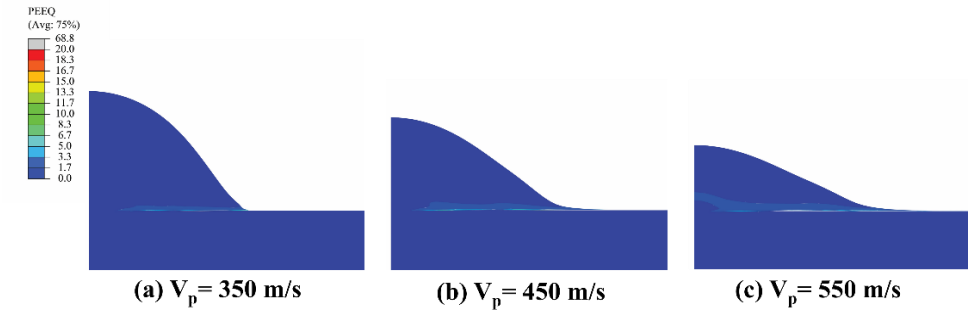

Figure 5. Simulation contour of PEEQ at 36ns of 25 µm Al particles upon an SKD11 hardening substrate at varying particle velocity (particle temperature at 623K)

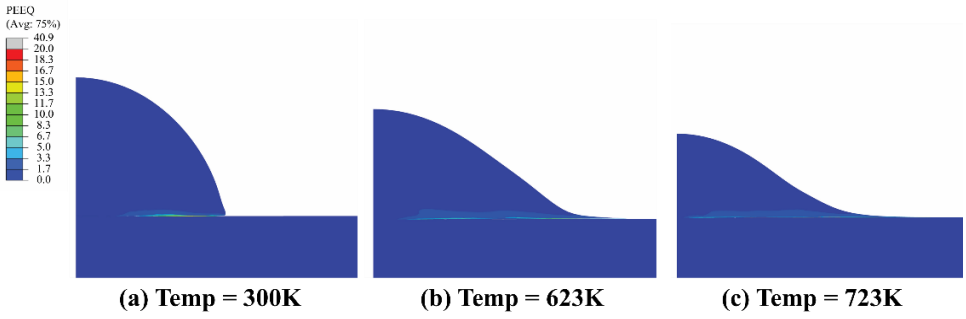

Figure 6. Simulation contour of PEEQ at 36ns of 25 µm Al particles upon an SKD11 hardening substrate at varying particle temperature (particle velocity at 450 m/s)

TABLE 2. Critical velocity of pure Al particle calculation from Equation 2

Initial particle temperature (K)	Critical velocity (m/s)
300	665
623	460
723	370

$$V_{cr} = 0.64\sqrt{\left(\frac{16\sigma_{TS}}{\rho_p\left(T_m - 293\right)} + C_p\right)\left[T_m - T_{pi}\right]} \quad (2)$$

where C_p is the particle-specific heat, T_m is the particle melting temperature, ρ_p is the particle density, σ_{TS} is the particle tensile strength, and T_{pi} is the particle impact temperature (28). The results are shown in Table 2.

The V_{cr} different temperatures could be estimated using Equation 2. For example, the particle velocity at 300K is approximately 665 m/s (see Table 2). It could be seen that V_{cr} decreases as particle temperature increases, as shown in Table 2. When considering the plastic strain equivalent (PEEQ) result, Figure 5 shows that the Al particles start adhering to the substrate at a particle velocity of 350 m/s, while the critical velocity determined by Equation 2 suggests a higher value of critical velocity. The deposition of soft particles onto a hard substrate typically demands a lower critical velocity, as demonstrated in the research conducted by Bae et al. (30). In their study, they determined that for scenarios involving particle sizes of 25 µm and a process temperature of 300K, the critical velocity was 775 m/s for Al particles on an Al substrate and 365 m/s for Al particles on a steel substrate. The current work observed that the critical velocity initiation occurred at approx. 400 m/s for 300K (see detail later in the text), which aligns with the work previously reported (30). This indicated that the simulated critical velocity was lower than the calculated value due to substrate effects. Specifically, when the substrate is harder than the particle, it has the potential to reduce the critical velocity.

It should be noted that the effect of particle size V_{cr} has also been discussed by Dowding et al. (37), suggesting increasing V_{cr} with decreasing particle size. This is because the small particle size has a higher surface area-to-volume ratio. It should be noted that Equation 2 does not include such an effect. The effect of particle size could be investigated in more detail using the current model to predict impact behavior.

The results of increasing temperature on the particle (see Figure 6) present the contour of PEEQ at the same particle velocity at various particle temperatures. The result shows that the particle increased surface area and deformed more when increasing particle temperature. Increasing the temperature of Al particles could result in particle softening and particles being easier to deform. Thus, an increase in particle temperature could increase particle flat length from 15 µm to 35 µm, 133% from its initial temperature (300K to 723K). This could also help in the deposition of the particle in the following impact.

Figure 7 provides a graph showing the relationship between plastic strain equivalent (PEEQ) and impact time for different particle temperatures. It could be seen that an increase in strain developed when increasing the temperature up to the melting point. With a process temperature equal to or higher than the melting temperature, the particle would start melting, and wetting phenomena may take place. Hence, Al material spreading out is expected. The deformation behavior of the particle, therefore, could result in a change in coating layer thickness depending on the particle geometry after impact.

4. 2. Effect of Particle Impact Velocity and Particle Temperature on Interface Temperature

Figure 8 (a)-(c) presents the temperature distribution in the particle and substrate during impact (at 36ns) for cases with an impact velocity of 450m/s. Figure 8(a) shows the result for an initial particle temperature of 300 K. It could be seen that the cohesive zone was small, and the temperature of a particle during impact at 36 ns was 823 K. The cohesive zone size increases by approximately 86% and 143%, and the temperature of a particle during impact at 36 ns rise to 1066 K and 1000K when the initial particle is 623 K and 723 K, respectively (see Figure 8b). The change in the cohesive zone and interface temperature could affect adhesion behavior,

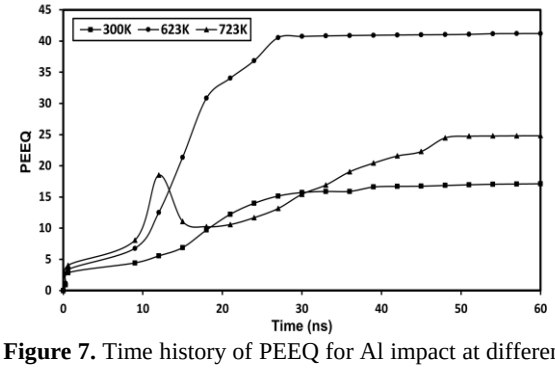

Figure 7. Time history of PEEQ for Al impact at different particle temperatures (Impact velocity of 450 m/s)

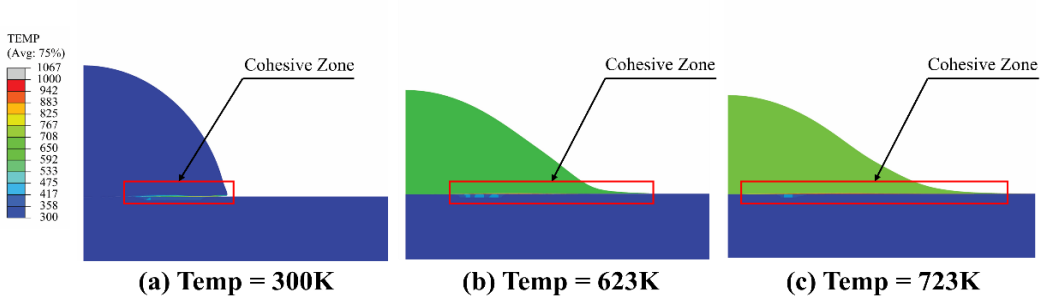

Figure 8. Temperature contour particle and substrate at 36ns, 450m/s with different particle temperatures

i.e., gap and adhesion strength, at the interface between the coating and the substrate. Figure 9 shows the relationship between particle temperatures at the interface with impact time for different initial particle temperatures. The particle temperature during impact would affect the particle deformation behavior during impact and in turn, result in a change in the critical velocity of Al particles as observed as a result of changing initial particle velocity, i.e., decreasing in the critical velocity is expected for higher initial particle velocity. As temperature rises, particles acquire greater kinetic energy, leading to increased vibrational intensity. As gas temperature increases, particles gain kinetic energy, resulting in higher speeds. Consequently, particles collide with surfaces more frequently and with greater impact.

4. 3. Influence of Particle Impact Velocity and Particle Temperature on Flattening Ratio The flattening ratio represents the severity of particle deformation after impact in a clearer aspect. Deposits with heavily deformed particles are likely to have less porosity, a high bonded area, and high cohesive strength, as described earlier. Thus, the flattening ratio can be examined as a "diagnostic" microstructure property. It acts as a benchmark for the general quality of cold-spray coating. Hence, the effect of particle impact on the flattening ratio is also investigated.

Figure 10 shows the typical characteristics of particles before and after impact. As the flattening ratio is closer to 1, less porosity is expected. This is because as the particles deformed flatter, the gap between the two colliding particles should be reduced, resulting in a denser coating.

On the other hand, the resulting coating will be highly porous if the flattening ratio is close to 0. In general, the elongation characteristics of a particle depend on particle velocity. High particle velocity results in a high flattening ratio. The flattening ratio can be calculated following Equation 4.

$$Flattening\ Ratio = 1 - \frac{h_p}{D_p} \quad (4)$$

where h_p is the height of the particle after impact and D_p is the diameter of the particle before impact.

For the flattening ratio, the relationship between the particle velocity and the flattening ratio can be plotted as shown in Figure 11, which shows the relationship between the particle velocity and the flattening ratio at different temperatures of the obtained coating predicted by the computational analysis. When increasing particle temperature, the flattening ratio increases to approximately 60% of room temperature. High particle velocity should be selected, or a flattening ratio approaching 1 should be chosen to reduce coating porosity and improve adhesion behavior. As shown in Figure 8, the flattening ratio, as indicated by the temperature contour, decreases as particle temperature increases, resulting in an expanded cohesive zone.

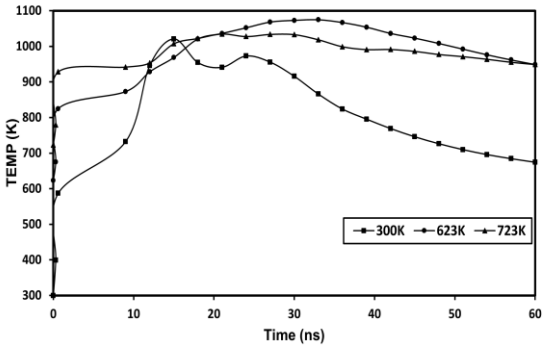

Figure 9. Time history of temperature for Al impact at different particle temperatures (Impact velocity of 450 m/s)

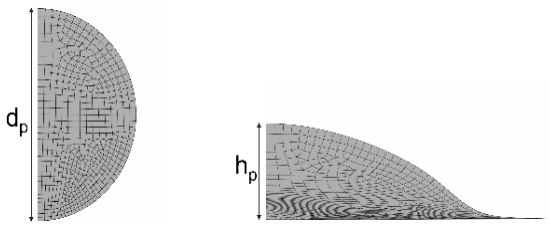

Figure 10. Characteristics of particles before and after impact on the substrate

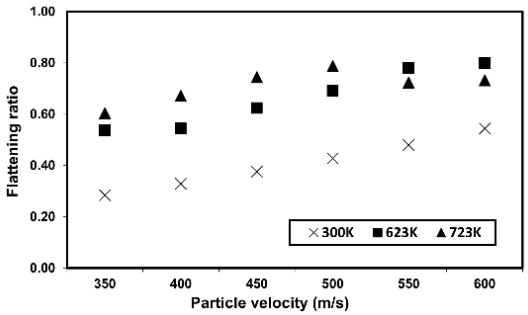

Figure 11. Relationship between the particle velocity and the flattening ratio at different temperatures

5. COLD SPRAY EXPERIMENT

To investigate the capability of the computational model, the experiment was performed. A process temperature of 623K was selected. The preliminary study of the cold spray of pure Al on SKD11 was first carried out. The pressure in the experiment could be determined by using the equation shown in Equation 5 (10) for a required particle velocity, V_p. The desired particle velocity was chosen based on computational results for 623K using the flattening ratio results. The particle velocity should be greater than the critical velocity, V_{cr}, which gives the flattening ratio greater than 0.5. Notably, the flattening ratio was approximately 0.5 when the particle velocity was equal to critical velocity $V_{cr}=V_p$ (28). This is to ensure that a coating with low porosity would be developed. The desired velocity of 450 m/s was selected.

$$V_p = \frac{1}{\frac{1}{M}\sqrt{\frac{M_{gas}}{\gamma RT}} + 0.85\sqrt{\frac{D}{x}}\sqrt{\frac{\rho_p}{P_0}}} \quad (5)$$

where M is the local Mach number and γ is the ratio of specific heat. For monatomic gases (He, Ar), γ is 1.66, and for diatomic gases (N_2, air), γ is typically 1.4. R is the gas constant (8314 J/kmol K). T is gas temperature. Local Mach number M only depends on the inner form of the nozzle. M_{gas} is the molecular weight of the gas used in the process. P_0 is the supply pressure measured at the entrance of the nozzle, while ρ_p is the particle density, D is the particle diameter, and x is the axial position.

The calculated pressure for the desired particle velocity is shown in Table 3a, while the particle velocity developed for a pressure of 1 MPa (the low pressure was chosen in this work due to the limitation of the CS machine) is shown in Table 3b. In Table 3b, the initial particle temperature affects the particle velocity in the process; as the temperature increases, particle velocity also increases. Temperature plays a significant role in adding energy to the spraying process in the form of heat. Elevated gas temperature enhances gas expansion through the nozzle, resulting in higher particle velocities. This observation is also related to the flattening ratio. Additionally, as the temperature increases, so does the temperature of the particles, leading to a greater degree of particle softening. This, in turn, increases the likelihood of plastic deformation during impact, ultimately improving deposition efficiency.

5. 1. Cold Spray of Pure Al Coating The characteristics of the sample after cold spray as shown in Figure 12. The sample was cross-sectioned by wire cutting to measure the thickness, as shown in Figure 13. The coating thickness was found to be 180±55 µm, while the hardness was 29.3±5 $HV_{0.1}$.

The preliminary experimental (pure Al) results confirmed that the computational model could be used to estimate the initial desired velocity, which was later used to select the process pressure for different particle temperatures based on particle deformation and interface behavior, i.e., flattening ratio. On the other hand, for a case with pressure limitation due to machine specification/performance, the required impact velocity for different particle temperatures could be estimated, which can be helpful in the design of the process parameters or improvement of the heating and pumping

TABLE 3a. Process pressure estimated for particle velocity of 450 m/s for different initial particle temperatures

Initial particle temperature (K)	Particle velocity	Pressure (MPa)
300	450	1.4
623	450	0.95
723	450	0.86

TABLE 3b. Particle velocity developed for a process pressure of 1 MPa for different initial particle temperatures

Initial particle temperature (K)	Pressure (MPa)	Particle velocity
300	1	387
623	1	457
723	1	471

Figure 12. Appearance of pure Al-coated specimen carried out at Impact-Innovations GmbH in Germany

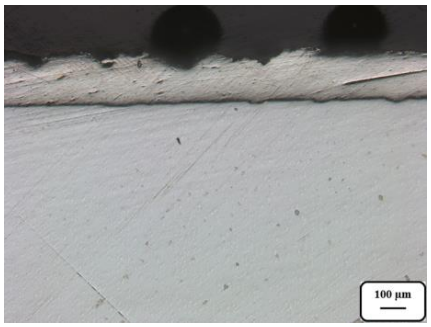

Figure 13. Optical micrographs for a cross-section of pure Al- coated specimen carried out at Impact-Innovations GmbH in Germany (magnitude 5x)

system. The effect of particle size should also be investigated with no major difficulty, which could be used as a guideline to reduce the process temperature and pressure.

5. 2. Cold Spray of Al/TiN Coating To improve the hardness of Al coating, TiN hard particles were added for reinforcement. To investigate the ability of the computational framework for the prediction of coating achievement based on Al particle impact behavior, the composite coatings deposition was performed. The selected size of TiN was smaller than pure Al to minimize the effect of TiN particles on Al particle flow and impact behavior. In this experiment, TiN was expected to disperse in a soft matrix and not deform. TiN particles are hard to deform or implant on a hard substrate at low velocity. The critical velocity and particle velocity of TiN (size 10 µm) could be estimated theoretically following the methodology previously described. The TiN critical velocity was approximately twice that of the Al particle, $V_{crAl,}$ and the particle velocity of TiN was approximately $1.2V_{pAl}$ (particle velocity of Al particle). Thus, TiN particles are expected to require higher energy for deformation on a hard substrate.

For the composite coating, the experiment used the same condition desired for pure Al (Pressure of 1 MPa, Temperature of 623K). Preliminary tests with 2 Al:TiN ratios (25 wt.% and 50 wt.% TiN) were investigated to study the upper limit of % TiN that could be deposited based on the critical velocity predicted for pure Al.

It was found that 50wt.% TiN was the limit of TiN fraction for conditions of pressure =1 MPa and temperature = 623K. It was also found that the average thickness of coating obtained for this case was approximately 18.7 ± 4.6µm, which was too thin, and the specimens were unevenly coated. This may be due to the effect of TiN particles on particle flow, which could reduce the travelling velocity and impact velocity of Al particles. It should be noted that the number of TiN particles is higher with a higher percentage of TiN. The micrograph presented in Figure 14 (a & b) shows an SEM (backscattered electron mode) micrograph of the cross-section of Al/TiN composite coating at a process temperature of 623K with magnitudes of 100x and 1000x, respectively.

A gap between the coating and substrate can be observed in Figure 14(b). The coating hardness was found to be 75.3 ±26.2 $HV_{0.1}$. The effect of the hard substrate could be expected due to the thin coating developed. Increasing the process pressure and temperature or reducing the TiN size may improve the coating process, resulting in an increase in coating thickness.

For a ratio of Al=75wt.%: TiN = 25%, the average coating thickness was found to be approximately 234.7 ± 51 µm, and the average coating hardness was 63.6 ±8.8 $HV_{0.1}$. Figure 15 presents a micrograph showing a cross-section of Al/TiN (fraction Al=75wt.%: TiN = 25wt.%).

The coating appears denser and thicker than that observed with a fraction of Al=50wt.%: TiN = 50wt.%. It could be said that the computational prediction of critical velocity and particle velocity of Al could be used for Al/TiN composite coating for the case with insignificant effect of TiN on Al impact behavior. Notably, the %TiN limitation is expected to be changed with process conditions and particle size. For this work, the TiN and Al particle sizes are 10 µm and 25 µm, respectively, and the process pressure and temperature are 1 MPa and 623K, respectively.

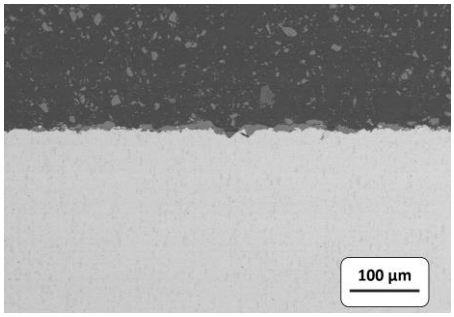

(a) magnitude 100x

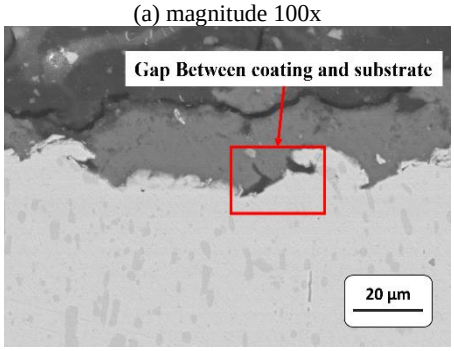

(b) magnitude 1000x

Figure 14. SEM (Back Scattered Electron mode with magnitude 100x and 1000x) micrograph showing a cross-section of Al/TiN (fraction Al=50wt.%: TiN = 50wt.%) (Centreline Center Line model SST PX)

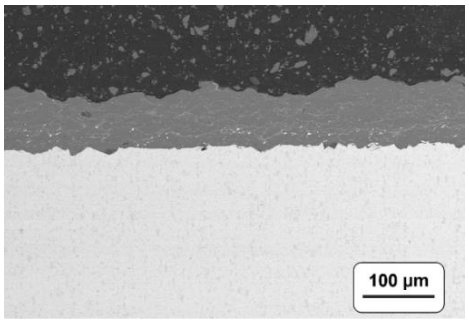

Figure 15. SEM (Back Scattered Electron mode with magnitude 100x) micrograph showing a cross-section of Al/TiN (fraction Al=75wt.%: TiN = 25wt.%) (Centreline Center Line model SST PX)

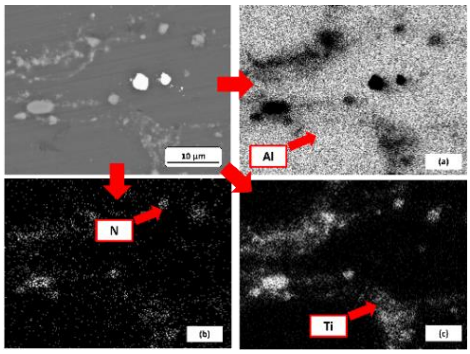

Figure 17. EDS mapping (Energy Dispersive Spectroscopy with magnitude 3000x) of the cold-sprayed Al/TiN composite coating at a process temperature of 723K.

For the experimental study of the effect of initial particle temperature, tests were performed at 623K and 723K for an Al:TiN ratio of 75 wt.%:25 wt.%. The pressure for both cases was fixed at 1 MPa.

A micrograph of Al/TiN composite coating in Figure 16 (a & b) shows an SEM (backscattered electron mode) micrograph of the cross-section of Al/TiN composite coating at process temperatures of 623K and 723K, respectively. The EDS mappings, as depicted in Figure 17, displayed the presence of pure aluminum (a) on the deposit side, along with nitrogen (b) and titanium (c).

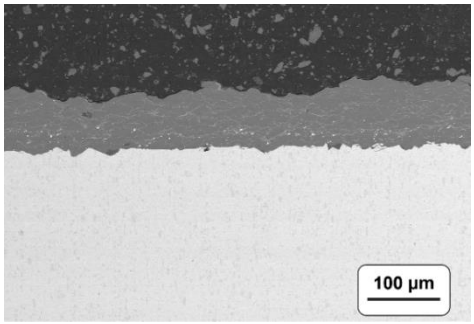

(a) Temperature at 623K

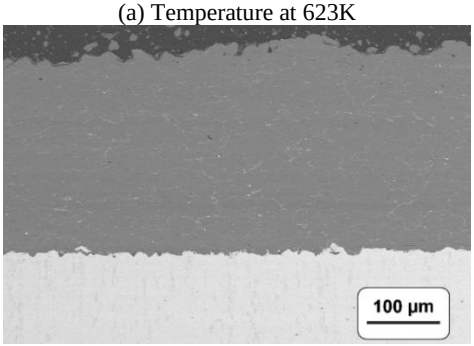

(b) Temperature at 723K

Figure 16. SEM (Back Scattered Electron mode with magnitude 100x) micrograph showing a cross-section of Al/TiN composite coating at different process temperatures (Centreline Center Line model SST PX)

The X-ray diffraction analysis of the Al/TiN composite coating was conducted, and the findings are presented in Figure 18. Based on the XRD analysis, the coating primarily consisted of aluminum (Al), with a limited presence of titanium nitride (TiN). The X-ray diffraction (XRD) analysis revealed the absence of impurities, additional phases, or significant phase alterations, thus confirming the absence of oxidation during the cold spray process. The results further confirmed the embedding of TiN particles within the Al matrix.

A micrograph showing a cross-section of Al/TiN reveals that the Al particles deformed flat and were deposited layer by layer. TiN particles were embedded around pure Al particles and were uniformly dispersed in the matrix (see Figure 19 (a)). Because the impact energy for particles of the soft component is high enough to adhere to the substrate, the impact energy of hard material is sufficient to adhere to the surface previously covered by soft material due to mechanical embedding (31). The volume fraction of TiN in the deposit was approximately 10% for both conditions. This differs slightly from the findings of Li et al. (24), who investigated TiN composite coating with high-pressure

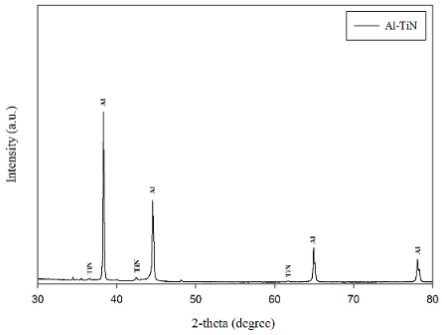

Figure 18. X-ray diffraction pattern of Al/TiN composite coating

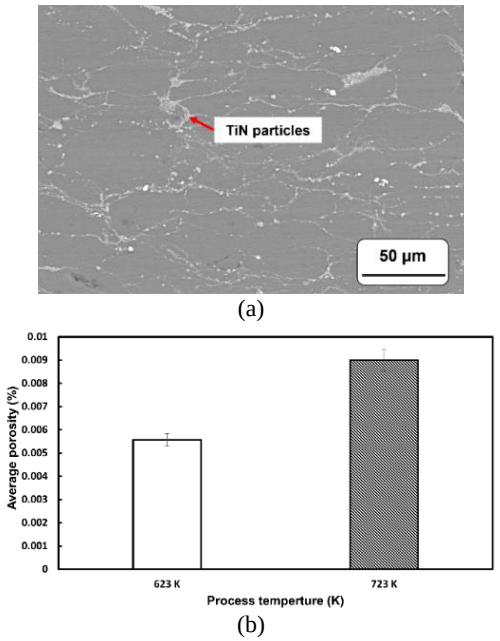

Figure 19. SEM (Back Scattered Electron mode with magnitude 500x) micrograph showing a cross-section of Al/TiN composite coating at a process temperature of 723K (a) and Al/TiN porous coating on SKD11 hardening by cold spraying (b)

cold spray at 25 wt.% TiN (resulting in a volume fraction of 13.9% in the deposit). It is evident that the flattening ratio results from simulations have utility in designing experimental conditions.

The results suggested that the temperature in the process affects coating porosity and thickness, as predicted by computational investigation. It was found that increasing the process temperature increases the thickness, and a dense Al/TiN composite coating was expected with this flattening ratio (> 0.5). The average percentage of voids was evaluated using IMAGE J analysis with SEM imagery. The result found that the porosity of the Al/TiN composite coating was less than 0.01% at both process temperatures (see Figure 19(b)). The results show that at a process temperature of 723 K, there is a higher percentage of porosity compared to 623 K. This observation may be attributed to the particle expansion and contraction behavior, as depicted in Figure 7 (Time history of PEEQ for Al impact at different particle temperatures (Impact velocity of 450 m/s)). At 723 K, particles initially expand from 0 to 10 seconds, then contract briefly before expanding again after 15 seconds. This cyclic behavior can create voids in the coating, resulting in a higher porosity at the higher process temperature of 723 K as compared to 623 K.

The coating thickness is presented in Figure 20. A higher particle temperature could increase particle velocity at the same process pressure, resulting in a thicker coating. This is because high particle velocity would result in flatter particles after impact, which could promote particles adhering during the impact of the following particle, i.e., the next particle layer.

The highest microhardness of Al/TiN composites was 74.2 ±6.5 $HV_{0.1}$ at 723 K. The hardness of the Al/TiN composite coating was higher than the Al deposit by 65% (the hardness of the pure Al deposit was 29.6 ±5.1 $HV_{0.1}$), as expected (23-25). Figure 21 shows that increasing the particle temperature could result in a coating with higher surface hardness. This is due to the effect of thicker coating with higher deformation obtained at higher temperatures, as the particles deform more easily, showing flatter particle geometry after each impact. The results align with those from Li et al. (24), who examined Al5356/TiN composite coating in high-pressure cold spray. They found that TiN particles increased the hardness of the matrix coating by 50%. For instance, with a TiN fraction of 25 wt.%, the hardness of Al5356/TiN reached approximately 140.38 $HV_{0.2}$, while Al5356 alone had a hardness of 68.7 $HV_{0.2}$. In terms of adhesive strength, Al5356 had a strength of 32 MPa, while Al5356/TiN exhibited an even higher strength exceeding 50 MPa (24, 25). Based on the Li et al. (24) study, the adhesive strength can be estimated to fall within the range of 30 MPa to 50 MPa. Note that this preliminary study did not include adhesive strength testing, but this aspect will be addressed in future work as the experimental conditions are refined.

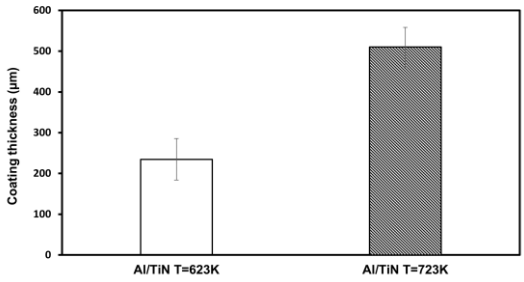

Figure 20. The average coating thickness of the composite coating

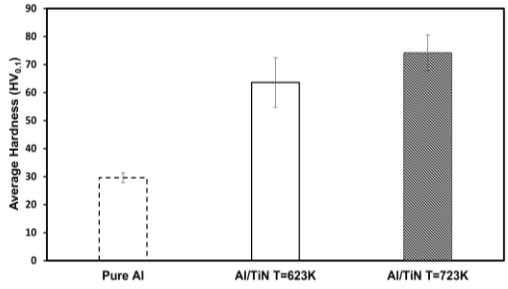

Figure 21. Average coating hardness of pure Al coating and composite coating

6. CONCLUSIONS

A simplified computational framework to predict the adherence of MMC coating was proposed, i.e. a model for a single impact of a single matrix particle. The deformation behavior of matrix particles could be investigated to provide information for CS process conditions to be selected for cases with the insignificant effect of hard reinforcement particles. The critical velocity, characteristic of particles during impact, and porosity in the coating could be predicted. Al/TiN coating was studied in this work. The effects of particle temperature and impact velocity were investigated. The results showed that:

- Single-shot particle impact modelling could be used to show representative composite coating deposition performance for the case of hard reinforcement particles as long as no significant effect of hard particles on matrix particle velocity is observed. For the Al/TiN coating studied in this work (TiN and Al particle sizes of approx. 10 μm and 25 μm, respectively), 25wt.% TiN was suggested.
- Particle temperature directly affects the cohesive zone; by increasing particle temperature, the cohesive zone area increases as well. This could confirm that the particles adhere to the substrate.
- The flattening ratio can be determined computationally, which can then be used as a guideline to predict the coating porosity.
- Particle deformation increases with increasing impact velocity and initial temperatures. Hence, the coating could be easier to deposit with higher particle velocity or higher initial temperature.

7. ACKNOWLEDGMENTS

The author would like to express the deepest appreciation to the Research and Researchers for Industries-RRI of the Thailand Research Fund and to Metalfine (Thailand) Ltd. for funding under the Research Scholar Grant (No.PHD59I0021 and RDG6150009). Sincere thanks are also extended to Professor Natasha Sacks at Stellenbosch University in South Africa for her advice and suggestions. Special thanks to the Material Manufacturing and Surface Engineering Research Center (MaSE lab) for providing laboratory support.

8. REFERENCES

1. Gapsari F, Hidayatia N, Setyarini P, Alan MP, Subagyo R, Andoko A. Hydroxyapatite coating on stainless steel 316l using flame spray technique. International Journal of Engineering, Transactions B: Applications. 2021;34(2):493-9. 10.5829/IJE.2021.34.02B.22
2. Afshar A, GHORBANI G, Ehsani N, Saeri M, Sorrell C. A STUDY OF ZETA POTENTIAL OF PLASMA SPRAYED HYDROXY AP ATITE COATING IN FOUR SIMULATED PHYSIOLOGICAL SOLUTIONS. International Journal of Engineering. 2003;16(4):343-54.
3. Ebrahimi N, Sedaghat Ahangari Hosseinzadeh A, Vaezi M, Mozafari M. Evaluation of corrosion resistance of bi-layered plasma-sprayed coating on titanium implants. International Journal of Engineering, Transactions A: Basics. 2022;35(4):635-43.
4. Poursaeidi E, Salarvand A. Comparison of properties of ti/tin/ticn/tialn film deposited by cathodic arc physical vapor and plasma-assisted chemical vapor deposition on custom 450 steel substrates. International Journal of Engineering, Transactions A: Basics. 2016;29(10):1459-68. 10.5829/idosi.ije.2016.29.10a.17
5. Nistratov AV, Klimenko NN, Pustynnikov IV, Vu LK. Thermal regeneration and reuse of carbon and glass fibers from waste composites. Emerg Sci J. 2022;6:967-84. 10.28991/ESJ-2022-06-05-04
6. Fauchais PL, Heberlein JV, Boulos MI. Thermal spray fundamentals: from powder to part: Springer Science & Business Media; 2014.
7. Khadayeir AA, Wannas AH, Yousif FH. Effect of Applying Cold Plasma on Structural, Antibacterial and Self Cleaning Properties of α-Fe2O3 (HEMATITE) Thin Film. Emerging Science Journal. 2022;6(1):75-85. 10.28991/ESJ-2022-06-01-06
8. Astuti P, Rafdinal RS, Yamamoto D, Andriamisaharimanana V, Hamada H. Effective Use of sacrificial zinc anode as a suitable repair method for severely damaged RC members due to chloride attack. Civil Engineering Journal. 2022;8(7):1535-48. 10.28991/CEJ-2022-08-07-015
9. Pawlowski L. The science and engineering of thermal spray coatings: John Wiley & Sons; 2008.
10. Huang R, Ma W, Fukanuma H. Development of ultra-strong adhesive strength coatings using cold spray. Surface and Coatings Technology. 2014;258:832-41. 10.1016/j.surfcoat.2014.07.074
11. Schmidt T, Gärtner F, Assadi H, Kreye H. Development of a generalized parameter window for cold spray deposition. Acta materialia. 2006;54(3):729-42. 10.1016/j.actamat.2005.10.005
12. Sansoucy E, Kim G, Moran A, Jodoin B. Mechanical characteristics of Al-Co-Ce coatings produced by the cold spray process. Journal of Thermal Spray Technology. 2007;16:651-60. 10.1007/s11666-007-9099-3
13. Huang R, Sone M, Ma W, Fukanuma H. The effects of heat treatment on the mechanical properties of cold-sprayed coatings. Surface and Coatings Technology. 2015;261:278-88. 10.1016/j.surfcoat.2014.11.017
14. Wu J, Fang H, Yoon S, Kim H, Lee C. Measurement of particle velocity and characterization of deposition in aluminum alloy kinetic spraying process. Applied surface science. 2005;252(5):1368-77. 10.1016/j.apsusc.2005.02.108
15. Moridi A, Hassani-Gangaraj SM, Guagliano M, Dao M. Cold spray coating: review of material systems and future perspectives. Surface Engineering. 2014;30(6):369-95. 10.1179/1743294414Y.0000000270
16. Hussain T. Cold spraying of titanium: a review of bonding mechanisms, microstructure and properties. Key engineering materials. 2013;533:53-90. 10.4028/www.scientific.net/KEM.533.53
17. Maev RG, Leshchynsky V. Low-pressure cold spray (LPCS). Cold-Spray Coatings: Recent Trends and Future perspectives. 2018:95-142. 10.1007/978-3-319-67183-3_4
18. Wang Q, Birbilis N, Zhang M-X. Process optimisation of cold spray Al coating on AZ91 alloy. Surface engineering. 2014;30(5):323-8. 10.1179/1743294413Y.0000000224

19. Irissou E, Legoux J-G, Arsenault B, Moreau C. Investigation of Al-Al2O3 cold spray coating formation and properties. Journal of Thermal Spray Technology. 2007;16(5-6):661-8. 10.1007/s11666-007-9086-8
20. Meng F, Hu D, Gao Y, Yue S, Song J. Cold-spray bonding mechanisms and deposition efficiency prediction for particle/substrate with distinct deformability. Materials & Design. 2016;109:503-10. 10.1016/j.matdes.2016.07.103
21. Hodder K, Nychka J, McDonald A. Comparison of 10 μm and 20 nm Al-Al 2 O 3 metal matrix composite coatings fabricated by low-pressure cold gas dynamic spraying. Journal of thermal spray technology. 2014;23:839-48. 10.1007/s11666-014-0094-1
22. Yu M, Li W. Metal matrix composite coatings by cold spray. Cold-Spray Coatings: Recent Trends and Future perspectives. 2018:297-318. 10.1007/978-3-319-67183-3_10
23. Li W-Y, Zhang G, Liao H, Coddet C. Characterizations of cold sprayed TiN particle reinforced Al2319 composite coating. journal of materials processing technology. 2008;202(1-3):508-13. 10.1016/j.jmatprotec.2007.09.045
24. Li WY, Zhang G, Guo X, Liao H, Coddet C. Characterizations of Cold-sprayed TiN Particle-reinforced Al Alloy-based Composites–from Structures to Tribological Behaviour. Advanced Engineering Materials. 2007;9(7):577-83. 10.1002/adem.200700085
25. Li W-Y, Zhang G, Zhang C, Elkedim O, Liao H, Coddet C. Effect of ball milling of feedstock powder on microstructure and properties of TiN particle-reinforced Al alloy-based composites fabricated by cold spraying. Journal of thermal spray technology. 2008;17:316-22. 10.1007/s11666-008-9182-4
26. Xie J, Nélias D, Walter-Le Berre H, Ogawa K, Ichikawa Y. Simulation of the cold spray particle deposition process. Journal of Tribology. 2015;137(4):041101. 10.1115/1.4030257
27. King PC BG, Zahiri SH, Jahedi M, Lee C. An experimental and finite element study of cold spray copper impact onto two aluminum substrates. Journal of thermal spray technology. 2010 19(4):620-34. 10.1007/s11666-009-9454-7
28. Assadi H, Schmidt T, Richter H, Kliemann J-O, Binder K, Gärtner F, et al. On parameter selection in cold spraying. Journal of thermal spray technology. 2011;20:1161-76. 10.1007/s11666-011-9662-9
29. Li W-Y, Zhang C, Li C-J, Liao H. Modeling aspects of high velocity impact of particles in cold spraying by explicit finite element analysis. Journal of Thermal Spray Technology. 2009;18:921-33. 10.1007/s11666-009-9325-2
30. Bae G, Xiong Y, Kumar S, Kang K, Lee C. General aspects of interface bonding in kinetic sprayed coatings. Acta Materialia. 2008;56(17):4858-68. 10.1016/j.actamat.2008.06.003
31. Sova A, Maestracci R, Jeandin M, Bertrand P, Smurov I. Kinetics of composite coating formation process in cold spray: Modelling and experimental validation. Surface and Coatings Technology. 2017;318:309-14. 10.1016/j.surfcoat.2016.06.084
32. Zhou H, Li C, Bennett C, Tanvir H, Li C. Numerical Analysis of Deformation Behavior and Interface Bonding of Ti6Al4V Particle After Subsequent Impact During Cold Spraying. Journal of Thermal Spray Technology. 2021;30:1093-106. 10.1007/s11666-021-01188-w
33. Yu M, Li W-Y, Wang F, Liao H. Finite element simulation of impacting behavior of particles in cold spraying by Eulerian approach. Journal of thermal spray technology. 2012;21:745-52. 10.1007/s11666-011-9717-y
34. Li J, Jing L, Chen M. An FEM study on residual stresses induced by high-speed end-milling of hardened steel SKD11. Journal of Materials Processing Technology. 2009;209(9):4515-20. 10.1016/j.jmatprotec.2008.10.042
35. Assadi H, Gärtner F, Stoltenhoff T, Kreye H. Bonding mechanism in cold gas spraying. Acta materialia. 2003;51(15):4379-94. 10.1016/S1359-6454(03)00274-X
36. Schmidt T, Assadi H, Gärtner F, Richter H, Stoltenhoff T, Kreye H, et al. From particle acceleration to impact and bonding in cold spraying. Journal of thermal spray technology. 2009;18:794-808. 10.1007/s11666-009-9357-7
37. Dowding I, Hassani M, Sun Y, Veysset D, Nelson KA, Schuh CA. Particle size effects in metallic microparticle impact-bonding. Acta Materialia. 2020;194:40-8. 10.1016/j.actamat.2020.04.044

Persian Abstract

چکیده

اسپری سرد (CS) با کامپوزیت زمینه فلزی (MMC) یک فرآیند جایگزین برای بهبود خواص سطحی است که در ساخت پلاستیک بسیار مهم است. درک رفتار ذرات در هنگام ضربه برای CS مورد نیاز است. این مطالعه بر توسعه یک چارچوب محاسباتی ساده شده با استفاده از مدل ضربه ذره تک شات برای پیش‌بینی پایبندی ذرات ماتریس در ضربه با سرعت پایین متمرکز بود. در این کار، SKD11 سخت پوشیده شده با کامپوزیت تقویت‌کننده ماتریس Al/TiN با هدف تأیید چارچوب پیشنهادی انتخاب شد. تاثیر ذرات Al در دماهای مختلف K ۳۰۰، K ۶۲۳ و K ۷۲۳ در محدوده سرعت پایین ۳۵۰–۶۰۰ متر بر ثانیه شبیه‌سازی شد، که نشان داد دمای ذرات بر ناحیه منسجم تأثیر می‌گذارد. با افزایش دمای ذرات، مناطق نیز با سرعت مشابه افزایش می‌یابند. نسبت مسطح شدن از شبیه سازی محاسبه شد و مشخص شد که تحت تأثیر سرعت ذرات قرار دارد. CS از Al و Al/TiN خالص (۷۵:۲۵ درصد وزنی) روی SKD11 سخت شده تحت K ۶۲۳ و K ۷۲۳ تحت آزمایش با فشار تخمین زده شده بر اساس نسبت مسطح و رفتار ذرات انجام شد. نتایج نشان می‌دهد که پوشش‌ها را می‌توان با استفاده از فشار تخمینی توسعه داد. پوشش Al/TiN در دماهای اولیه ذرات مختلف رسوب داده شد. نتایج نشان می دهد که تخلخل پوشش کم (<۰.۰۱٪) را می توان برای هر دو مورد به دست آورد، و دمای ذرات بالاتر ضخامت و درصد تخلخل بیشتری را نشان می دهد، که به خوبی با نتایج محاسباتی مطابقت دارد. چارچوب توسعه‌یافته پتانسیل بالایی برای طراحی CS برای پوشش MMC نشان می‌دهد، مشروط بر اینکه ذرات تقویت‌کننده به طور قابل‌توجهی بر جریان ذرات ماتریس یا شرایط ضربه تأثیر نگذارند.